Space Vector Taylor-Fourier Models for Synchrophasor, Frequency and ROCOF Measurements in Three-Phase Systems

Paolo Castello, *Member, IEEE,* Roberto Ferrero, *Senior Member, IEEE,* Paolo Attilio Pegoraro, *Member, IEEE,* Sergio Toscani, *Member, IEEE*

Abstract

Taylor-Fourier (TF) filters represent a powerful tool to design PMU algorithms able to estimate synchrophasor, frequency and rate of change of frequency (ROCOF). The resulting techniques are based on dynamic representations of the synchrophasor, hence they are particularly suitable to track the evolution of its parameters during time-varying conditions. Electrical quantities in power systems are typically three-phase and weakly unbalanced, but most PMU measurement techniques are developed by considering them as a set of three single-phase signals; on the contrary, this peculiarity can be favorably exploited to improve accuracy and reduce the computational cost. In this respect, the present paper proposes to directly perform the TF expansion of the space vector (SV) samples obtained from three-phase measurements. A new paradigm allows to independently estimate positive and negative sequence synchrophasors along with system frequency and ROCOF, leveraging the three-phase characteristics. Performance of the proposed technique is assessed by using test signals inspired by standard IEEE C37.118.1-2011, including noise as well as magnitude and phase unbalance. Achieved results highlight the flexibility of the enhanced SV-based approach, which is capable to combine excellent dynamic performance together with accurate estimation of both positive and negative sequence components.

Index Terms

Phasor Measurement Unit (PMU), Synchrophasor estimation, Frequency, Rate of Change of Frequency (ROCOF), Voltage Measurement.

I. Introduction

Phasor Measurement Units (PMUs) are synchronized devices intended to measure amplitude, phase angle, frequency and rate of change of frequency (ROCOF) of electrical signals in power networks. Initially designed for transmission networks [1], they are expected to become a widespread tool also in electric distribution systems, being considered as promising to pave the implementation of smart grids [2] able to automatically control the network operation based on an accurate, fast and reliable monitoring.

PMUs label data with time-tags referred to a common timescale (the coordinated universal time, UTC, obtained from a GPS receiver is typically adopted), so that measurements collected on a wide area can be correlated and employed even in real-time, thus enabling an accurate representation of the operating conditions that can be exploited in grid control applications [2].

PMU algorithms are designed to extract the fundamental frequency component, along with the corresponding frequency and ROCOF, coping with different conditions that may occur in electrical signals: dynamics, harmonic and interharmonic disturbances, rapid variations, etc.

Several algorithms have been proposed in recent literature (see [2] for a review), based on a wide range of estimation techniques and tailored according to specific test conditions. Signal dynamics is particularly important, since PMUs are designed to operate even at high reporting rates (50 frames/s or even higher in 50 Hz systems) in order to track amplitude, phase angle and frequency changes. The last standard for synchrophasor measurements IEEE C37.118.1-2011 [3] (along with its amendment [4]) introduces the concept of dynamic synchrophasor and prescribes specific tests that can be representative of both slow variations, like amplitude or phase angle modulations and linear frequency ramps, and abrupt changes, such as amplitude and phase angle steps. Limits in terms of accuracy or dynamic response are reported for the different test conditions.

An interesting approach to measure dynamic signal parameters was proposed in [5] where a Taylor expansion of the phasor around the measurement instant is adopted to better describe its time evolution (Taylor-Fourier approach, TF), thus allowing a more accurate dynamic tracking of the related quantities. Such model has been exploited by different algorithms. In [6], [7], for instance, estimations are based on the discrete Fourier transform (DFT) and the model is employed to correct them by

P. Castello and P. A. Pegoraro are with the Department of Electrical and Electronic Engineering, University of Cagliari, 09123 Cagliari, Italy (e-mail: paolo.castello@diee.unica.it; paolo.pegoraro@diee.unica.it)

R. Ferrero is with the Department of Electrical Engineering and Electronics, University of Liverpool, Liverpool L69 3GJ, U.K. (e-mail: roberto.ferrero@liverpool.ac.uk).

S. Toscani is with the Dipartimento di Elettronica, Informazione e Bioingegneria, Politecnico di Milano, 20133 Milan, Italy (e-mail: sergio.toscani@polimi.it).

(c) 2019 IEEE. Personal use of this material is permitted. Permission from IEEE must be obtained for all other users, including reprinting/republishing this material for advertising or promotional purposes, creating new collective works for resale or redistribution to servers or lists, or reuse of any copyrighted components of this work in other works. DOI:10.1109/TIM.2019.2905747 Publisher version:https://ieeexplore.ieee.org/document/8684272

considering the effects due to parameter variations. In [8] the Taylor expansion approach is used to extend the interpolated DFT algorithm, while in [9] a two-channel PMU algorithm based on a Taylor approach is employed to achieve simultaneous compliance with P and M classes requirements defined by [3], [4].

All the above algorithms are designed starting from a single-phase signal. Recently, the idea of exploiting the typical characteristics of three-phase quantities to define PMU algorithms has been proposed. In particular, in [10] a space vector (SV) based algorithm is introduced. The positive sequence synchrophasor is obtained from the SV by means of an IIR filtering stage and two least-squares FIR interpolators: a first one for amplitude estimation and a second one allowing phase angle and frequency measurements. In [11], all the quantities are derived by FIR filtering the real and imaginary parts of the SV. In particular, frequency and ROCOF are obtained by applying properly-designed first and second order partial-band FIR differentiators, respectively, which allow designing algorithms that are compliant with the performance classes defined in [3] and [4]. In [12], the SV transformation is considered as a preliminary stage for the Interpolated DFT computation, thus allowing better estimations under off-nominal frequency conditions.

Other works exploiting similar approaches can be found in the literature. As an example, [13] and [14] use the SV transformation on a stationary reference frame in order to estimate the positive sequence phasor. On the contrary, [15] measure the positive sequence synchrophasor with respect to a rotating reference frame, which provides three-phase demodulation.

In [16] conventional TF filtering and the SV approach are combined in order to permit the estimation of positive and negative sequence synchrophasors, frequency and ROCOF that characterize three-phase signals with considerable reduction in terms of computational burden.

It should be noticed that positive and negative sequence components have very different magnitudes during typical operation; a first consequence is that the challenge to be faced when they have to be extracted from the complex SV signal are extremely different in the two cases. On the one hand negative component measurement may suffer from severe spectral interference due to the positive sequence term acting as a very large disturbance that have to be suppressed with strong filtering. On the other hand, dynamic performance is much more important as far as the positive sequence synchrophasor estimate. Furthermore, since the spectrum of the SV signal is far from being hermitian, there is no reason to design TF filters having the same expansion order for the positive and negative sequence terms.

Starting from the previous considerations, this paper proposes a radically new approach using completely different TF filters for positive and negative sequence estimations; in turns, these filter may be characterized by different expansion orders for the positive and negative sequence components. The additional degrees of freedom in filter design allow a more effective exploitation of the three-phase peculiarities of electrical signals. For example, the proposed technique allows to finely tune the filters to achieve an accurate and prompt detection of unbalance [17], which is key to avoid severe contingencies and blackouts [18].

The proposed approach is validated and discussed by means of simulations intended to show the impact of the TF filter design parameters on the overall measurement accuracy. This allows highlighting the advantages and the generality of the proposed framework for PMU algorithm design.

II. Taylor-Fourier Approach in Three-phase Systems

A. Conventional Taylor-Fourier Synchrophasor Estimation

As stated in the introduction, dynamic phasor measurements through Taylor-Fourier filtering were proposed in [5] to accurately track slow transients of electrical signals in ac power system applications. In several works, this approach has been exploited to design PMU algorithms having remarkable dynamic performance. The first step is writing the synchrophasor model: supposing operation near the rated frequency f_0 (corresponding to the angular frequency ω_0), the time evolutions of its real and imaginary parts are slow in the common, UTC-synchronized reference frame rotating at the angular speed ω_0. Therefore they can be represented with truncated Taylor expansions (up to the Kth order) around the generic measurement instant t_r:

$$\bar{x}(t-t_r) \simeq \sum_{k=0}^{K} \bar{X}^{(k)}(t_r)\frac{(t-t_r)^k}{k!} \tag{1}$$

where $\bar{x}(t-t_r)$ is the dynamic synchrophasor while $\bar{X}^{(k)}(t_r)$ represents its kth derivative in the measurement instant. The previous expression can be rewritten by using the vector notation. To this purpose, let us introduce the complex column vector $\bar{\mathbf{p}}_K(t_r)$ of the phasor derivatives and the real row vector $\mathbf{a}$:

$$\bar{\mathbf{p}}_K(t_r) = \left[\begin{array}{cccc} \bar{X}^{(0)}(t_r) & \bar{X}^{(1)}(t_r) & \cdots & \bar{X}^{(K)}(t_r) \end{array}\right]^{\mathsf{T}} \tag{2}$$

$$\mathbf{a}(t-t_r) = \left[\begin{array}{cccc} 1 & t-t_r & \cdots & \frac{(t-t_r)^K}{K!} \end{array}\right] \tag{3}$$

where ^{T} denotes the transpose operator.

Therefore:

$$\bar{x}(t-t_r) \simeq \mathbf{a}(t-t_r)\bar{\mathbf{p}}_K(t_r) \tag{4}$$

The time domain expression of the signal can be obtained by projecting its synchrophasor on the real axis of a stationary reference frame, as we do when the inverse Steinmetz transform is applied to a phasor:

$$x(t-t_r) \simeq \sqrt{2}\Re\left[\mathbf{a}(t-t_r)\bar{\mathbf{p}}_K(t_r)e^{j\omega_0(t-t_r)}\right] \tag{5}$$

denoting with * the complex conjugate operator, (5) can be rewritten in a more convenient form[1]:

$$\begin{aligned} &x(t-t_r) = \\ &= \left[\begin{array}{cc} \mathbf{a}(t-t_r)e^{j\omega_0(t-t_r)} & \mathbf{a}(t-t_r)e^{-j\omega_0(t-t_r)} \end{array}\right] \frac{\bar{\mathbf{p}}(t_r)}{\sqrt{2}} \end{aligned} \tag{6}$$

where $\bar{\mathbf{p}}(t_r)$ is defined as:

$$\bar{\mathbf{p}}(t_r) = \left[\begin{array}{c} \bar{\mathbf{p}}_K(t_r) \\ \bar{\mathbf{p}}_K^*(t_r) \end{array}\right] \tag{7}$$

It is evident that, in general, the time domain expression is a non-holomorphic function of the $K+1$ synchrophasor derivatives in the measurement instant t_r, since it involves also their complex conjugates. Estimating the synchrophasor means inverting (6), but it is an underdetermined problem: at least $2K+2$ independent constraints are required. To this purpose, let us suppose to have available a N-sample window (N odd and greater than $2K+2$) of the time domain waveform centered in t_r. Assuming that such samples are collected with a uniform interval T_s, low enough to avoid aliasing artifacts, they can be arranged in a column vector $\mathbf{x}(t_r)$:

$$\mathbf{x}(t_r) = \left[\begin{array}{c} x(t_r + \frac{N-1}{2})T_s \\ \vdots \\ x(t_r - \frac{N-1}{2})T_s \end{array}\right] \tag{8}$$

and the following system of equations can be set up:

$$\mathbf{x}(t_r) = \frac{1}{\sqrt{2}}\left[\bar{\mathbf{\Phi}}\mathbf{A} \;\; \bar{\mathbf{\Phi}}^*\mathbf{A}\right]\bar{\mathbf{p}}(t_r) = \frac{1}{\sqrt{2}}\bar{\mathbf{B}}\bar{\mathbf{p}}(t_r) \tag{9}$$

where:

$$\mathbf{A} = \left[\begin{array}{c} \mathbf{a}(\frac{N-1}{2}T_s) \\ \vdots \\ \mathbf{a}(-\frac{N-1}{2}T_s) \end{array}\right] \tag{10}$$

$$\bar{\mathbf{\Phi}} = \left[\begin{array}{ccccc} e^{j\omega_0\frac{N-1}{2}T_s} & & & & \\ & \ddots & & & \\ & & 1 & & \\ & & & \ddots & \\ & & & & e^{-j\omega_0\frac{N-1}{2}T_s} \end{array}\right] \tag{11}$$

The synchrophasor and its derivatives can be obtained by minimizing the norm of the error between model output and waveform samples. It requires computing the matrix $\bar{\mathbf{H}}$ as the pseudoinverse of $\bar{\mathbf{B}}$:

$$\hat{\bar{\mathbf{p}}}(t_r) = \sqrt{2}(\bar{\mathbf{B}}^{\mathsf{H}}\bar{\mathbf{B}})^{-1}\bar{\mathbf{B}}^{\mathsf{H}}\mathbf{x}(t_r) = \sqrt{2}\bar{\mathbf{H}}\mathbf{x}(t_r) \tag{12}$$

where ^{H} denotes the Hermitian transpose operator while $\hat{}$ indicates that the quantity is an estimate. From (12) it can be noticed that, with this approach, measuring the synchrophasor and its derivatives is a linear operation, corresponding to apply a bank of FIR filters of length N (the rows of matrix $\sqrt{2}\bar{\mathbf{H}}$, two for each derivative order including the zeroth) to the time-domain signal. The order K of the expansion and the window length N are the design parameters that allow tailoring their frequency response functions in order to match specific requirements. In turn, frequency and ROCOF estimates are provided by the following formulas, that require at first and second order expansions, respectively:

[1]The equality symbol is used instead of similarity symbol from here on for the sake of simplicity, thus assuming that the model holds true.

$$\hat{f}(t_r) = f_0 + \frac{1}{2\pi} \frac{\Im\left[\hat{\bar{X}}_p^{(1)}(t_r) \cdot \hat{\bar{X}}_p^{(0)*}(t_r)\right]}{\left|\hat{\bar{X}}_p^{(0)}(t_r)\right|^2}$$

$$\widehat{\text{ROCOF}}(t_r) = \frac{1}{\pi}\left(\frac{\Im\left[\hat{\bar{X}}_p^{(2)}(t_r)\bar{X}_p^{(0)*}(t_r)\right]}{2\left|\hat{\bar{X}}_p^{(0)}(t_r)\right|^2} + \right.$$

$$\left. - \frac{\Re\left[\hat{\bar{X}}_p^{(1)}(t_r)\hat{\bar{X}}_p^{(0)*}(t_r)\right]\Im\left[\hat{\bar{X}}_p^{(1)}(t_r)\hat{\bar{X}}_p^{(0)*}(t_r)\right]}{\left|\hat{\bar{X}}_p^{(0)}(t_r)\right|^4}\right) \tag{13}$$

A closer look at (12) allows several, interesting considerations. Reminding (7), it returns not only the synchrophasor derivatives (first $K+1$ rows of $\hat{\bar{\mathbf{p}}}(t_r)$), but also their complex conjugates (last $K+1$ rows of $\hat{\bar{\mathbf{p}}}(t_r)$), which is redundant information. Another closely related issue is that the estimates of the synchrophasor and its derivatives are affected by interference due to the dynamic image component when the synchrophasor model is not exact.

B. Straightforward Extension to Three-phase Systems

For both economic and technical reasons, ac power systems are inherently three-phase. For a given electrical quantity, the Taylor-Fourier estimator (12) can be straightforwardly applied to each of the three phases; adopting a matrix formulation is more convenient. To the purpose, let us define the matrixes $\mathbf{X}_{abc}(t_r)$ and $\bar{\mathbf{P}}_{abc}(t_r)$ containing the samples and the syncrophasor derivatives of the three phases, respectively:

$$\mathbf{X}_{abc}^{\mathsf{T}}(t_r) = \begin{bmatrix} \mathbf{x}_a^{\mathsf{T}}(t_r) \\ \mathbf{x}_b^{\mathsf{T}}(t_r) \\ \mathbf{x}_c^{\mathsf{T}}(t_r) \end{bmatrix} \qquad \bar{\mathbf{P}}_{abc}^{\mathsf{T}}(t_r) = \begin{bmatrix} \bar{\mathbf{p}}_a^{\mathsf{T}}(t_r) \\ \bar{\mathbf{p}}_b^{\mathsf{T}}(t_r) \\ \bar{\mathbf{p}}_c^{\mathsf{T}}(t_r) \end{bmatrix} \tag{14}$$

where the subscript a, b or c indentifies a particular phase. In this way, the three-phase model can be easily written:

$$\mathbf{X}_{abc}^{\mathsf{T}}(t_r) = \frac{1}{\sqrt{2}}\bar{\mathbf{P}}_{abc}^{\mathsf{T}}(t_r)\bar{\mathbf{B}}^{\mathsf{T}} \tag{15}$$

and it can be inverted in a least squares (LS) sense to obtain the estimates of the synchrophasor, their derivatives and their conjugates:

$$\hat{\bar{\mathbf{P}}}_{abc}^{\mathsf{T}}(t_r) = \sqrt{2}\mathbf{X}_{abc}^{\mathsf{T}}(t_r)\bar{\mathbf{H}}^{\mathsf{T}} \tag{16}$$

This formulation maintains all the drawbacks of the single-phase implementation. Furthermore, different frequency and ROCOF estimations can be performed by applying (13) to each of the three phases (see also [16]. However, a unique frequency and ROCOF has to be provided for a three-phase quantity. A straightforward yet inefficient possibility is computing the mean of the three single-phase estimates.

C. Symmetrical Components and Taylor-Fourier Filters

The analysis of three-phase systems is much more effective when carried out by using the symmetrical components. To this purpose, let us define the transformation matrix $\bar{\mathbf{S}}$ that allows obtaining the symmetrical components from the three phasors ($\bar{\alpha} \triangleq e^{j2\pi/3}$):

$$\bar{\mathbf{S}} = \frac{1}{\sqrt{3}}\begin{bmatrix} 1 & \bar{\alpha} & \bar{\alpha}^2 \\ 1 & \bar{\alpha}^2 & \bar{\alpha} \\ 1 & 1 & 1 \end{bmatrix} \tag{17}$$

With this formulation $\bar{\mathbf{S}}$ is unitary, hence its inverse corresponds to the Hermitian transpose $\bar{\mathbf{S}}^{\mathsf{H}}$. The symmetrical components transformation can be applied to the matrix $\hat{\bar{\mathbf{P}}}_{abc}^{\mathsf{T}}(t_r)$:

$$\hat{\bar{\mathbf{P}}}_S^{\mathsf{T}}(t_r) = \bar{\mathbf{S}}\bar{\mathbf{P}}_{abc}^{\mathsf{T}}(t_r) = \sqrt{2}\bar{\mathbf{S}}\mathbf{X}_{abc}^{\mathsf{T}}(t_r)\bar{\mathbf{H}}^{\mathsf{T}} \tag{18}$$

and, by performing simple considerations, it can be noticed that the resulting matrix $\hat{\bar{\mathbf{P}}}_S^{\mathsf{T}}(t_r)$ shows the following structure:

$$\hat{\bar{\mathbf{P}}}_S^{\mathsf{T}}(t_r) = \begin{bmatrix} \hat{\bar{\mathbf{p}}}_+^{\mathsf{T}}(t_r) & \hat{\bar{\mathbf{p}}}_-^{*\mathsf{T}}(t_r) \\ \hat{\bar{\mathbf{p}}}_-^{\mathsf{T}}(t_r) & \hat{\bar{\mathbf{p}}}_+^{*\mathsf{T}}(t_r) \\ \hat{\bar{\mathbf{p}}}_0^{\mathsf{T}}(t_r) & \hat{\bar{\mathbf{p}}}_0^{*\mathsf{T}}(t_r) \end{bmatrix} \tag{19}$$

where $\hat{\bar{\mathbf{p}}}_s(t_r)$ with $s \in \{+, -, 0\}$ is the column vector containing the estimates of the positive, negative or zero sequence synchrophasors together with the corresponding K derivatives. Hence, adopting the usual notation:

$$\hat{\bar{\mathbf{p}}}_s(t_r) = \begin{bmatrix} \hat{\bar{X}}_s^{(0)}(t_r) & \hat{\bar{X}}_s^{(1)}(t_r) & \cdots & \hat{\bar{X}}_s^{(K)}(t_r) \end{bmatrix}^{\mathsf{T}} \tag{20}$$

where $\hat{\bar{X}}_s^{(k)}(t_r)$ is the generic sequence p synchrophasor kth derivative.

Looking at (19) it becomes evident that the first two rows of $\hat{\bar{\mathbf{p}}}_s(t_r)$ carry the same information. In particular, when the zero sequence component is *a priori* negligible or not present (e.g. line voltages), the first row synthesize all the parameters describing the dynamic phasors of the three-phase quantity. Using (17), (18), (19) it can be written:

$$\begin{bmatrix} \hat{\bar{\mathbf{p}}}_+^{\mathsf{T}}(t_r) & \hat{\bar{\mathbf{p}}}_-^{*\mathsf{T}}(t_r) \end{bmatrix} = \sqrt{\frac{2}{3}} \begin{bmatrix} 1 & \bar{\alpha} & \bar{\alpha}^2 \end{bmatrix} \mathbf{X}_{abc}^{\mathsf{T}}(t_r) \bar{\mathbf{H}}^{\mathsf{T}} \tag{21}$$

In (21) the N samples of the SV related to the three phase quantity can be recognized. Defining:

$$\hat{\bar{\mathbf{p}}}_{SV}(t_r) = \begin{bmatrix} \hat{\bar{\mathbf{p}}}_+(t_r) \\ \hat{\bar{\mathbf{p}}}_-^*(t_r) \end{bmatrix} \tag{22}$$

$$\bar{\mathbf{x}}_{SV}^{\mathsf{T}}(t_r) = \sqrt{\frac{2}{3}} \begin{bmatrix} 1 & \bar{\alpha} & \bar{\alpha}^2 \end{bmatrix} \mathbf{X}_{abc}^{\mathsf{T}}(t_r) \tag{23}$$

therefore (21) can be expressed as:

$$\hat{\bar{\mathbf{p}}}_{SV}(t_r) = \bar{\mathbf{H}} \bar{\mathbf{x}}_{SV}(t_r) \tag{24}$$

The previous equation applies the Taylor-Fourier expansion to the SV signal, performed by inverting the following expression in the LS sense:

$$\bar{\mathbf{x}}_{SV}(t_r) = \bar{\mathbf{B}} \bar{\mathbf{p}}_{SV}(t_r) \tag{25}$$

This approach features many advantages with respect to separately processing the phase signals as in the previous subsection. First of all, no redundant data is returned by (24), since, when looking at the SV, it is a linear, holomorphic function of the positive and the conjugate of the negative sequence synchrophasors. Several applications only require to measure the positive sequence synchrophasor: in this way it is directly obtained with clear advantages in terms of computational cost, since three single-phase estimations are avoided. Furthermore, frequency and ROCOF of a three-phase quantity are typically obtained starting from the time evolution of the phase angle of the fundamental, positive sequence synchrophasor. In fact, the reference P and M class methods proposed by [3], [4] adopt this definition. Finally, it should be noticed that the positive sequence synchrophasor carries most of the information about the three-phase quantity because of the typically weak unbalance levels in power systems. Therefore, supposing that the phase signals are purely sinusoidal, the estimate of the positive sequence synchrophasor is only affected by interference with the negative sequence component, which is surely much lower in amplitude. In this respect, a single-phase estimation is much more critical, since it may suffer from interaction with the large image component.

D. Taylor Fourier Filters of the Space Vector

In the previous paragraph, it has been shown how the positive and negative sequence synchrophasors (and their derivatives) can be estimated by applying a Kth order Taylor-Fourier filter bank to the SV samples. The results are the same as those obtained by performing three Taylor-Fourier transforms of the single-phase signals (with the same order K) and then computing the symmetrical components thanks to the Fortescue transformation; however, the computational burden is considerably reduced. On the other hand, starting from single-phase quantities implies that the expansion orders of the positive and negative sequence synchrophasors must be the same. This constraint can be removed by thinking in terms of SV signal while reminding the relationship with positive and negative sequence dynamic synchrophasors, modeled with K_+ and K_- expansion orders respectively. Therefore, let us define:

$$\bar{\mathbf{p}}_s(t_r) = \begin{bmatrix} \bar{X}_s^{(0)}(t_r) & \bar{X}_s^{(1)}(t_r) & \cdots & \bar{X}_s^{(K_s)}(t_r) \end{bmatrix}^{\mathsf{T}} \tag{26}$$

$$\mathbf{a}_s(t - t_r) = \begin{bmatrix} 1 & t - t_r & \cdots & \frac{(t-t_r)^{K_s}}{K_s!} \end{bmatrix} \tag{27}$$

with $s \in \{+,-\}$. Using the relationship between symmetrical components synchrophasors and SV, the model results:

$$\bar{x}_{SV}(t-t_r) = \mathbf{a}_+(t-t_r)\bar{\mathbf{p}}_+(t_r)e^{j\omega_0(t-t_r)} + \\ + \mathbf{a}_-(t-t_r)\bar{\mathbf{p}}_-^*(t_r)e^{-j\omega_0(t-t_r)} = \\ = \left[\begin{array}{cc} \mathbf{a}_+(t-t_r)e^{j\omega_0(t-t_r)} & \mathbf{a}_-(t-t_r)e^{-j\omega_0(t-t_r)} \end{array}\right] \bar{\mathbf{p}}_{SV}(t_r) \quad (28)$$

where the last term is obtained introducing $\bar{\mathbf{p}}_{SV}(t_r) \triangleq \left[\begin{array}{cc} \bar{\mathbf{p}}_+^{\mathsf{T}}(t_r) & \bar{\mathbf{p}}_-^{\mathsf{H}}(t_r) \end{array}\right]^{\mathsf{T}}$ and defining $\bar{\mathbf{x}}_{SV}(t_r)$ (N sample window of the SV signal centered in t_r) as in (22) and (23):

$$\bar{\mathbf{x}}_{SV}(t_r) = \left[\bar{\mathbf{\Phi}}\mathbf{A}_+ \;\; \bar{\mathbf{\Phi}}^*\mathbf{A}_-\right] \bar{\mathbf{p}}_{SV}(t_r) = \bar{\mathbf{B}}_\pm \bar{\mathbf{p}}_{SV}(t_r) \quad (29)$$

where:

$$\mathbf{A}_s = \left[\begin{array}{c} \mathbf{a}_s(\frac{N-1}{2}T_s) \\ \vdots \\ \mathbf{a}_s(-\frac{N-1}{2}T_s) \end{array}\right] \quad (30)$$

with $s \in \{+,-\}$. Assuming that the usual hypothesis are met and that $N \geq K_+ + K_- + 2$, the previous problem is overderdetermined and $\bar{\mathbf{B}}_\pm$ has a left pseudoinverse $\bar{\mathbf{H}}_\pm$ so that (29) can be solved in the least squares sense as follows:

$$\bar{\mathbf{p}}_{SV}(t_r) = \bar{\mathbf{H}}_\pm \bar{\mathbf{x}}_{SV}(t_r) = \left(\bar{\mathbf{B}}_\pm^{\mathsf{H}}\bar{\mathbf{B}}_\pm\right)^{-1} \bar{\mathbf{x}}_{SV}(t_r) \quad (31)$$

$\bar{\mathbf{H}}_\pm$ contains the bank of FIR filters that allows obtaining $\hat{\bar{\mathbf{p}}}_{SV}$ (namely the estimate of $\bar{\mathbf{p}}_{SV}$) for each window of SV samples, being (24) formally identycal to (31). The first $K_+ + 1$ rows of $\bar{\mathbf{H}}_\pm$ allow computing the positive sequence synchrophasor (and its derivatives) while the last $K_- + 1$ rows permit evaluating the conjugate of the negative sequence synchrophasor (together with its derivatives).

Now, it should be noticed that the challenges to be faced when the positive or negative sequence synchrophasor have to be measured are very different. For example, the signal to noise ratio and the spectral interference may heavily affect the estimation of the negative sequence component, while their impact is not so pronounced as for the positive sequence synchrophasor measurement. On the one hand, if frequency and ROCOF have to be measured, at least a second order expansion of the positive sequence synchrophasor is required; on the other hand this is not mandatory as far as the negative sequence synchrophasor. Furthermore, good dynamic performance is needed to follow the evolution of the positive sequence synchrophasor, while usually it does not apply to the negative sequence synchrophasor. It should be noticed that generally increasing the order of the expansion allows better dynamic performance (flatter bandpass) but at the expense of lower frequency selectivity, which makes the estimate more sensitive to spectral interference and broadband noise.

Therefore, an interesting solution that allows a more flexible tuning of the algorithm is to employ different models (thus different Taylor Fourier expansion orders) for estimating the positive and the negative synchrophasor. Thanks to the proposed approach, it is possible to choose a couple of expansion orders K_{++} and K_{+-} that will be used to obtain the filters for estimating the positive sequence synchrophasor and its two first derivatives (first three rows of the resulting pseudoinverse $\mathbf{H}_+$). At the same time, a potentially different couple of expansion orders K_{-+} and K_{--} can be employed to compute the filters for estimating the (conjugate of the) negative sequence synchrophasor (namely the first row of the pseudoinverse $\mathbf{H}_-$).

III. Tests and Results

Hybrid SV-TF algorithms proposed in Section II-D have been tested and compared by means of numerical simulations under Matlab environment. A sampling frequency $f_s = 10$ kHz is adopted and a 50-Hz system is considered ($f_0 = 50$ Hz). Synchronization error is neglected since it would affect every algorithm in the same way, namely producing a phase-angle error due to the clock offset (typical GPS time error is < 100 ns and timebase error $< 1\,\mu$s).

Different TF filters can be defined according to the selected expansion orders (namely K_{++} and K_{+-} when focusing on the positive-sequence estimation) and window length. In the following, the smallest odd number of samples including an integer number of nominal cycles is used.

Synchrophasor, frequency and ROCOF are evaluated sample-by-sample as if a reporting rate equal to f_s were considered. The performance of the algorithms is quantified and expressed in terms of total vector error (TVE) %, absolute frequency error (FE) and absolute ROCOF error (RFE) for synchrophasor, frequency and ROCOF estimations, respectively, as defined by [3].

Algorithms are tested with different input signals, covering both steady-state and dynamic conditions; maximum TVE, FE and RFE are computed in each test. Since the aim is assessing algorithm performance and highlighting the impact of design parameters, the test signals are only inspired by those of the compliance tests in IEEE C37.118.1 (and IEEE C37.118.1a) [3], [4], without in any way claiming to be exhaustive with respect to P or M class requirements. While in [16] the focus was about the advantages of a three-phase TF implementation, in this paper the generalization of the model allowed by the SV approach is considered in order to show how the additional degrees of freedom can be exploited. According to this purpose,

it is more useful to test the algorithm performance under specific yet realistic conditions, thus including also the presence of noise and unbalance which are typically neglected by the relevant standards.

Firstly, following the achievements of Section II, a dynamic test is performed. Three-phase, amplitude modulated signals are applied; sinusoidal modulation having frequency $f_m \in [0, 5]$ Hz (with a step of 0.1 Hz) is adopted. The generic expression of the test signal is given by:

$$\mathbf{x}_{abc}(t) = \sqrt{2}X\left(1 + x_m(t)\right) \cdot \Re\left(e^{j2\pi f_0 t}\begin{bmatrix} 1 & \bar{\alpha}^2 & \bar{\alpha} \end{bmatrix}^{\mathsf{T}}\right) \tag{32}$$

where $\mathbf{x}_{abc}(t)$ is the vector of phase signals, X is the common rms magnitude and:

$$x_m(t) = k_x \cos\left(2\pi f_m t\right) \tag{33}$$

k_x represents the amplitude modulation depth; the highest value considered by [4] has been adopted, thus $k_x = 0.1$.

Table I shows the maximum TVE (for positive sequence synchrophasor estimation), FE and RFE values for two modulation frequency ranges ($[0, 2]$ Hz and $[0, 5]$ Hz, respectively) when the algorithm is implemented with different positive sequence expansion orders; window lengths corresponding to 2 or 3 nominal cycles are used. The negative sequence component is either expanded to the same order as the positive one ($K_{+-} = K_{++}$) or excluded from the model. All the errors are low and only slight advantages are obtained by increasing K_{++}. It is interesting to notice that considering the negative sequence component does not give significant improvements. This perfectly reflects the considerations performed in Section II, since when a balanced three-phase input is acquired, no negative sequence component is present and thus, a single-sideband SV signal model holds. The slight improvement achieved by including also the negative sequence contribution is due to undermodeling: the model error due to the truncated TF expansion is partially embedded by the negative sequence term.

TABLE I
MAXIMUM TVE, FE, RFE UNDER AMPLITUDE MODULATION

max f_m	**Orders**		**Cycles**	**TVE** [%]	**FE** [mHz]	**ROCOF** [Hz/s]
	K_{++}	K_{+-}				
2	2	2	2	$1.4 \cdot 10^{-4}$	$3.0 \cdot 10^{-3}$	$1.9 \cdot 10^{-3}$
	2	-	2	$1.6 \cdot 10^{-4}$	~0	~0
	3	3	2	$1.4 \cdot 10^{-4}$	$2.3 \cdot 10^{-3}$	$3.3 \cdot 10^{-5}$
	3	-	2	$1.6 \cdot 10^{-4}$	~0	~0
	4	4	2	$8.2 \cdot 10^{-7}$	$0.9 \cdot 10^{-5}$	$1.5 \cdot 10^{-4}$
	4	-	2	$0.9 \cdot 10^{-7}$	~0	~0
	2	2	3	$0.8 \cdot 10^{-3}$	$3.3 \cdot 10^{-3}$	$1.5 \cdot 10^{-3}$
	2	-	3	$0.8 \cdot 10^{-3}$	~0	~0
	3	3	3	$0.7 \cdot 10^{-3}$	$2.7 \cdot 10^{-3}$	$4.3 \cdot 10^{-5}$
	3	-	3	$0.8 \cdot 10^{-3}$	~0	~0
	4	4	3	$0.1 \cdot 10^{-5}$	$3.0 \cdot 10^{-5}$	$4.1 \cdot 10^{-5}$
	4	-	3	$0.1 \cdot 10^{-5}$	~0	~0
5	2	2	2	$5.4 \cdot 10^{-3}$	0.12	$3.1 \cdot 10^{-2}$
	2	-	2	$6.2 \cdot 10^{-3}$	~0	~0
	3	3	2	$5.3 \cdot 10^{-3}$	0.09	$3.2 \cdot 10^{-3}$
	3	-	2	$6.2 \cdot 10^{-3}$	~0	~0
	4	4	2	$7.9 \cdot 10^{-5}$	$2.3 \cdot 10^{-3}$	$1.4 \cdot 10^{-2}$
	4	-	2	$2.1 \cdot 10^{-5}$	~0	~0
	2	2	3	$2.9 \cdot 10^{-2}$	0.12	$2.3 \cdot 10^{-2}$
	2	-	3	$3.0 \cdot 10^{-2}$	~0	~0
	3	3	3	$2.8 \cdot 10^{-2}$	0.12	$4.1 \cdot 10^{-3}$
	3	-	3	$3.0 \cdot 10^{-2}$	~0	~0
	4	4	3	$0.2 \cdot 10^{-3}$	$7 \cdot 10^{-3}$	$3.8 \cdot 10^{-3}$
	4	-	3	$0.2 \cdot 10^{-3}$	~0	~0

Similar results can be obtained when phase angle modulation is considered. The modulating signal is still sinusoidal and its frequency f_m in swept in the same ranges as before. Table II shows that there are significant values only for FE and RFE, particularly when higher modulation frequencies are considered. Results reflect the above discussion, since errors are very

similar notwithstanding the different models adopted. Once again, measurement improvements are linked to the order of K_{++}, which extends the filters bandwidths.

TABLE II
MAXIMUM TVE, FE, RFE UNDER PHASE MODULATION

max f_m	**Orders**		**Cycles**	**TVE** [%]	**FE** [mHz]	**ROCOF** [Hz/s]
	K_{++}	K_{+-}				
2	2	2	2	$1.7 \cdot 10^{-4}$	1.2	$1.1 \cdot 10^{-2}$
	2	-	2	$1.5 \cdot 10^{-4}$	1.3	$1.1 \cdot 10^{-2}$
	3	3	2	$1.3 \cdot 10^{-4}$	$2.0 \cdot 10^{-3}$	$1.1 \cdot 10^{-2}$
	3	-	2	$1.5 \cdot 10^{-4}$	$1.6 \cdot 10^{-3}$	$1.1 \cdot 10^{-2}$
	4	4	2	$9.8 \cdot 10^{-7}$	$1.3 \cdot 10^{-3}$	$1.1 \cdot 10^{-4}$
	4	-	2	$1.3 \cdot 10^{-7}$	$1.8 \cdot 10^{-3}$	$0.1 \cdot 10^{-4}$
	2	2	3	$7.2 \cdot 10^{-3}$	2.8	$2.5 \cdot 10^{-2}$
	2	-	3	$7.5 \cdot 10^{-4}$	2.9	$2.6 \cdot 10^{-2}$
	3	3	3	$6.9 \cdot 10^{-4}$	$8.3 \cdot 10^{-3}$	$2.4 \cdot 10^{-2}$
	3	-	3	$7.5 \cdot 10^{-4}$	$8.2 \cdot 10^{-3}$	$2.6 \cdot 10^{-2}$
	4	4	3	$1.5 \cdot 10^{-6}$	$7.9 \cdot 10^{-3}$	$7.1 \cdot 10^{-5}$
	4	-	3	$1.4 \cdot 10^{-6}$	$7.9 \cdot 10^{-3}$	$5.5 \cdot 10^{-5}$
5	2	2	2	$5.0 \cdot 10^{-3}$	19	0.42
	2	-	2	$5.8 \cdot 10^{-3}$	20	0.44
	3	3	2	$4.9 \cdot 10^{-3}$	0.14	0.41
	3	-	2	$5.8 \cdot 10^{-3}$	0.16	0.44
	4	4	2	$1.0 \cdot 10^{-4}$	0.13	$1.1 \cdot 10^{-2}$
	4	-	2	$0.3 \cdot 10^{-4}$	0.17	$0.3 \cdot 10^{-2}$
	2	2	3	$2.7 \cdot 10^{-2}$	42	0.96
	2	-	3	$2.8 \cdot 10^{-2}$	43	0.98
	3	3	3	$2.6 \cdot 10^{-2}$	0.74	0.94
	3	-	3	$2.8 \cdot 10^{-2}$	0.78	0.98
	4	4	3	$2.6 \cdot 10^{-4}$	0.75	0.13
	4	-	3	$3.4 \cdot 10^{-4}$	0.83	0.14

It should be noticed that the choice of the TF expansion orders have significant impact in the presence of broadband noise which typically affects the samples. Figs. 1 and 2 show the results when steady-state signals at the rated frequency with superimposed uniform noise are applied. The root mean square errors of frequency and ROCOF estimations ($\mathrm{FE}_{\mathrm{rms}}$ and $\mathrm{RFE}_{\mathrm{rms}}$, respectively) are reported at increasing noise levels, with signal to noise ratios (SNRs) in the range $40 \div 90$ dB. Typical SNR values of acquired signals are between 60 and 80 dB (e.g. 72 dB corresponds to 12 effective bits) but sometimes they can be even lower [19]. A wider range has been explored in order to study the behavior also in case of extremely good or very poor signal to noise ratio. $\mathrm{FE}_{\mathrm{rms}}$ and $\mathrm{RFE}_{\mathrm{rms}}$ are employed since maximum errors can be highly uncertain because of noise. The analysis is focused on a 2-cycle window and K_{++} values of 2 and 4 are considered.

For all the test cases, errors decrease by including only the positive sequence term in the SV model. The reduction of $\mathrm{FE}_{\mathrm{rms}}$ ranges from $5.8\,\%$ for order 2 to $13.3\,\%$ for order 4, while that of $\mathrm{RFE}_{\mathrm{rms}}$ is about $6.8\,\%$ for order 2 and $29.6\,\%$ for order 4. Smaller improvements can be achieved also for TVE (up to $7.1\,\%$), but they are not reported for the sake of brevity. As expected, wideband noise rejection is strictly linked to the equivalent noise bandwidth of each filter, thus using different expansions orders for positive and negative sequence terms allows enhancing robustness with respect to noise.

All together, the reported results show that thanks to the flexibility of the proposed approach it is possible to follow the positive sequence synchrophasor, frequency and ROCOF dynamics while also guaranteeing a better immunity to disturbances. These considerations apply to all the tests of the standard IEEE C37.118.1 [3], since PMU compliance tests are designed only for positive-sequence signals.

Now, it is very interesting to investigate the performance achieved with unbalanced three-phase signals which may occur in real-world applications, in particular when distribution systems are considered. Tests were performed at both nominal and off-nominal frequency with different types of unbalance. Since standards [3], [4] consider only positive sequence signals, these tests have been inspired by the unbalanced signals suggested in the guide IEEE C37.242 [20]. The following single-phase variations are applied:

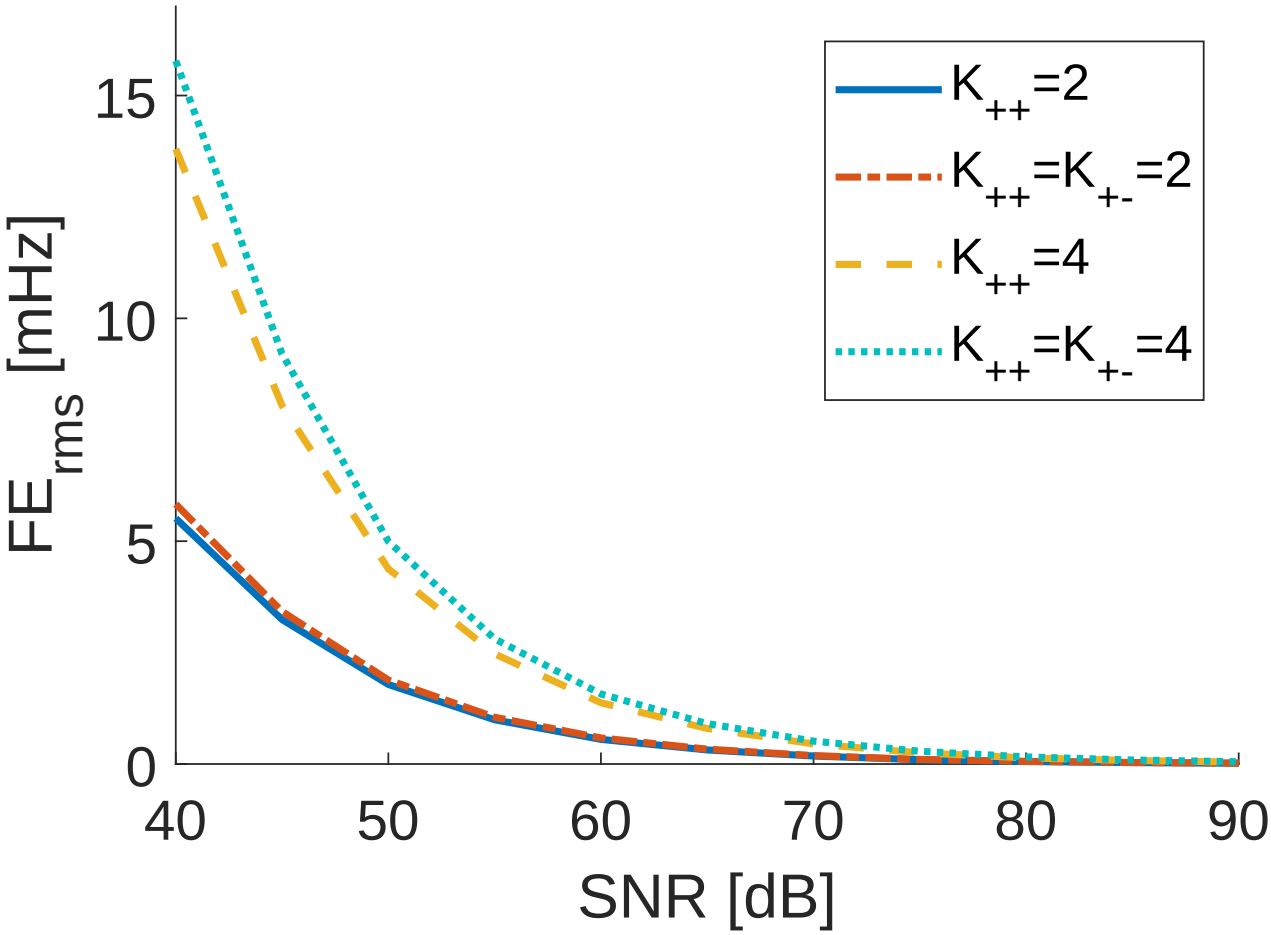

Fig. 1. Impact of broadband noise: root mean square FE achieved by SV-TF with different expansion orders.

- Magnitude variations δ_m: $\pm 10\,\%$ (corresponding to unbalance levels of $3.2\,\%$ and $3.4\,\%$)
- Phase-angle variations δ_ϕ: $\pm 10°$ (corresponding to an unbalance level of $5.8\,\%$)

where $(1+\delta_m)$ and δ_ϕ are, respectively, the amplification factor and the phase angle deviation applied to phase a. Table III reports the maximum TVE, FE and RFE for two frequencies and $\delta_m = +10\,\%$ when different orders are used (2-cycle algorithms). 49 Hz and 50 Hz frequencies are considered, as suggested by [20]. It is clear that a purely positive-sequence model $K_{++} > 0$ is no longer sufficient to match the SV and thus the errors become unacceptable. On the other end, a first order expansion ($K_{+-} = 1$) is suitable to properly consider the negative sequence component even under off-nominal frequency conditions.

Since TF filtering is based on least squares fitting, more accurate estimations are achieved when the model is able to match the actual signal. In Figs. 3 and 4 the $\mathrm{FE_{rms}}$ and $\mathrm{RFE_{rms}}$ results for a $+10\,\%$ magnitude variation with a $60\,\mathrm{dB}$ noise are considered in the frequency range $[49, 51]$ Hz. In particular, the errors for $K_{++} = 4$ are reported with different values of K_{+-}. The configuration $\{K_{++}, K_{+-}\} = \{4, 1\}$ gives best results for both FE and RFE with maximum error reductions with respect to the configuration $\{4, 4\}$ of about $12\,\%$ and $29\,\%$, respectively. It is possible to notice that the advantages with respect to the configuration $\{4, 2\}$ become less relevant as the frequency offset increases; the reason lies in the trade-off between stopband flatness around $-f_0$ (that allows reucing interference with the negative sequence term) and wideband noise filtering. Similar results have been obtained for $\mathrm{TVE_{rms}}$, but error reduction is lower (~$7\,\%$). Fig. 5 reports the results for a $10°$ variation of phase a signal (only $\mathrm{RFE_{rms}}$ is reported for the sake of brevity); the previous considerations for amplitude unbalance apply also in this case. The advantages of $\{4, 1\}$ are evident for frequencies close to f_0 ($\mathrm{RFE_{rms}}$ reduces up to $29\,\%$); when a larger frequency deviation occurs, the effect of the negative sequence infiltration becomes more important, hence a larger K_{+-} (e.g. 2) allows reducing its impact.

The algorithm presented in Section II also permits to estimate the negative sequence synchrophasor. In this context the definition of the SV model becomes even more important, since, as explained in previous sections, $\bar{X}_-$ is much lower than $\bar{X}_+$, thus resulting in a increased sensitivity to interference with the positive sequence term and disturbances. Table IV shows

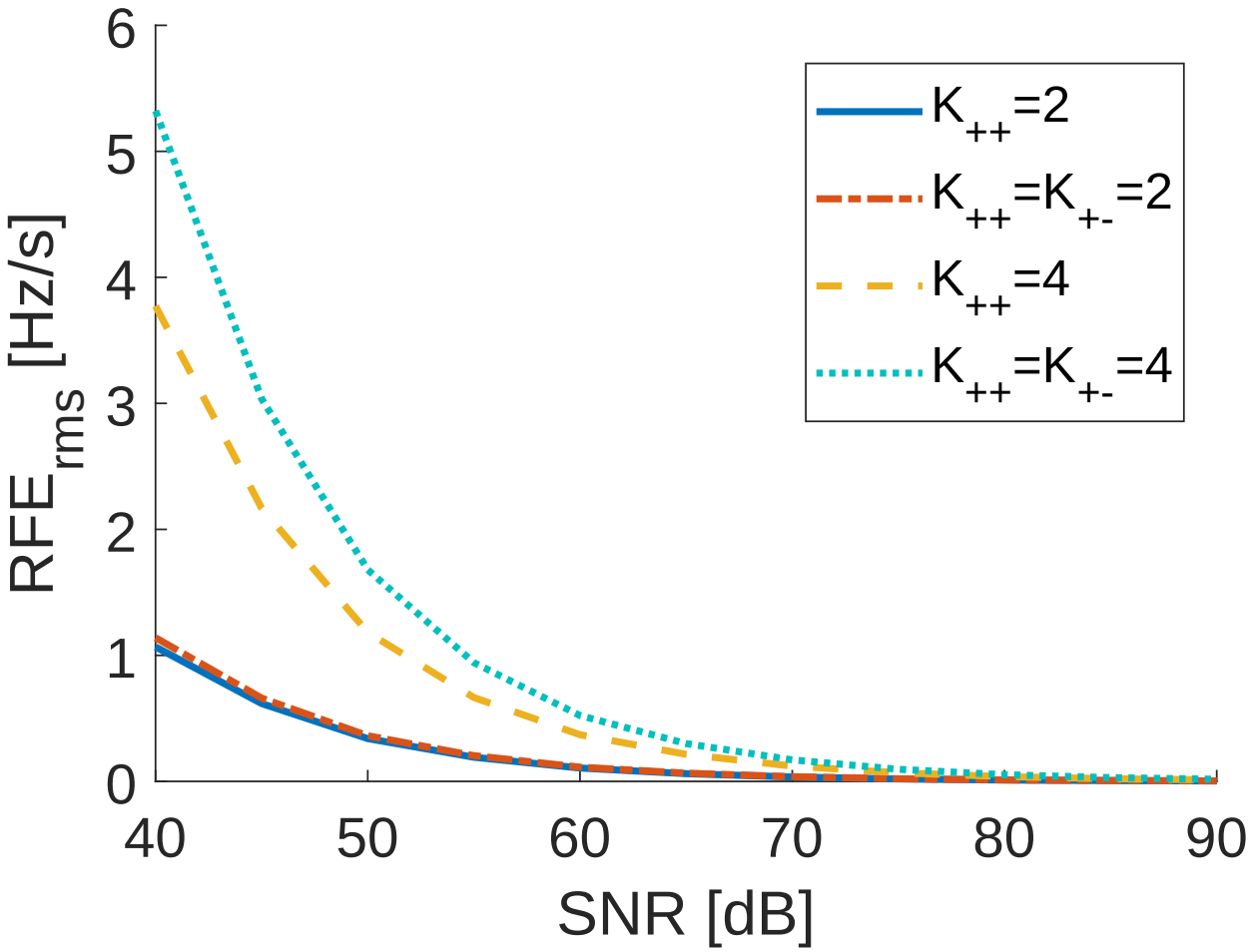

Fig. 2. Impact of broadband noise: root mean square RFE achieved by SV-TF with different expansion orders.

TABLE III
MAXIMUM TVE, FE, RFE UNDER MAGNITUDE UNBALANCE ($\delta_m = +10\,\%$)

frequency	**Orders**		**TVE** [%]	**FE** [mHz]	**ROCOF** [Hz/s]
	K_{++}	K_{+-}			
50	2	2	~0	~0	~0
	2	1	~0	~0	~0
	2	-	0.16	61	4.0
	4	4	~0	~0	~0
	4	1	~0	~0	~0
	4	-	0.49	130	48.2
49	2	2	$1.1 \cdot 10^{-4}$	1.5	$1.6 \cdot 10^{-3}$
	2	1	$1.5 \cdot 10^{-3}$	1.9	$3.6 \cdot 10^{-2}$
	2	-	0.12	62	1.5
	4	4	$2.8 \cdot 10^{-7}$	$3.7 \cdot 10^{-7}$	$2.2 \cdot 10^{-7}$
	4	1	$2.5 \cdot 10^{-3}$	$4.5 \cdot 10^{-4}$	$1.3 \cdot 10^{-4}$
	4	-	0.47	138	42.8

the $\mathrm{TVE_{rms}}$ values for the negative sequence estimation (2-cycle window) in the above conditions ($\delta_m = +10\,\%$ and SNR $= 60\,\mathrm{dB}$) for different $\{K_{-+}, K_{--}\}$ couples. It is important to notice that, as expected, TVE values are much higher than those considering positive sequence measurements. Choosing a suitable filter configuration has a dramatic impact on the accuracy: with $\{4, 1\}$, for instance, it is possible to get at least a $30\,\%$ error reduction at the rated frequency with respect to configurations

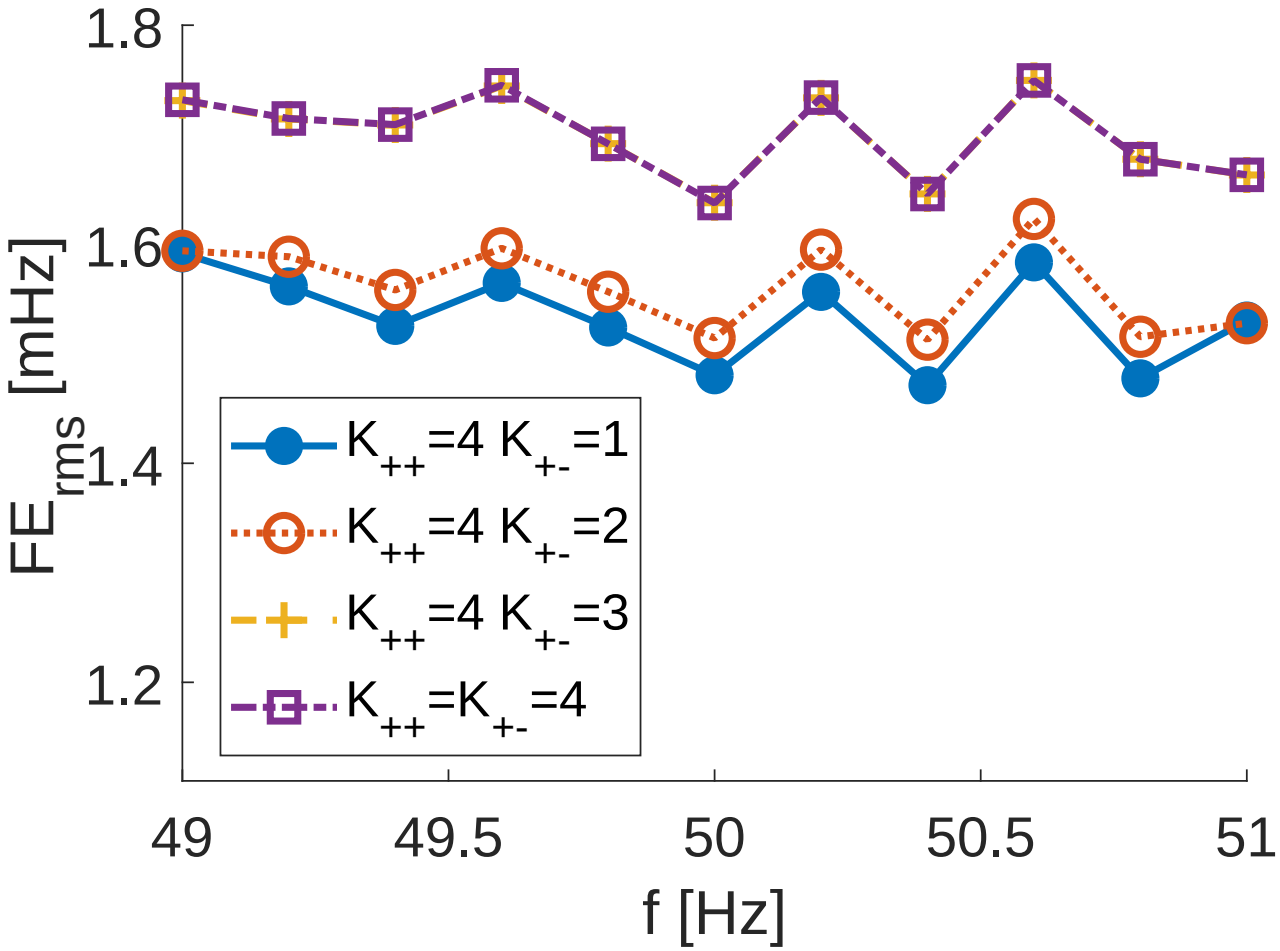

Fig. 3. Root mean square FE achieved by SV-TF with different negative sequence component expansion orders under magnitude unbalance, 60 dB SNR.

resulting in similar TVE errors at 49 Hz.

The accuracy in estimating the negative sequence synchrophasor have been compared to that achieved by using the well-known standard P-class method (P-C37.118.1) in [3] having the same two-cycle length. The negative sequence synchrophasor has been obtained by applying the Fortescue transformation to the estimated single-phase synchrophasors. For the above magnitude unbalance at 49 Hz, with a SNR $= 60\,\mathrm{dB}$, P-C37.118.1 results in $\mathrm{RFE}_{\mathrm{rms}} \simeq 0.860$ Hz/s and $\mathrm{TVE}_{\mathrm{rms}} \simeq 0.383\,\%$ for the negative sequence synchrophasor, which is much larger than almost all the configurations listed in Table IV. From another viewpoint, it is important to recall that the standard P-class method achieves maximum TVE errors which are at least two orders of magnitude larger than those reported in Tables I and II under amplitude and phase modulations.

Finally, tests have been performed also by considering signals acquired with a real data acquisition stage. Since real-world signals lack of ground-truth reference, algorithms are verified by using signals generated with an OMICRON CMC256Plus calibrator [21] synchronized with the IRIG-B output of CMIRIG-B interface [22] fed by a GPS receiver ($\pm 1\,\mu$s overall synchronization accuracy). A typical PMU input level of 100 Vrms is used as reference voltage and thus a 300 Vrms NI-9225 card [23] is employed with $f_s = 50$ kHz. As an example, the results in terms of $\mathrm{FE}_{\mathrm{rms}}$, for the $+10\%$ magnitude unbalance and 49 Hz frequency, are 0.6 mHz and 1.2 mHz for the configurations $\{K_{++}, K_{+-}\} = \{4, 1\}$ and $\{4, 4\}$, respectively. These values fully confirm the considerations derived from simulation results in Fig. 3. It is important to recall that the calibrator gives a stable frequency with a 0.5 ppm accuracy, corresponding to less that 0.025 mHz at nominal frequency.

IV. Conclusions

In this paper, a general framework to merge two powerful approaches (TF and SV) for PMU algorithm design in three-phase systems has been presented.

TF filters have been applied to estimate the positive and negative sequence synchrophasors from the time domain samples obtained by applying the SV transformation. The proposed technique allows an independent estimation of the positive and negative sequences components by exploiting different Taylor expansions. This represents a very important outcome since the measurement challenges to be faced in the two cases are completely different.

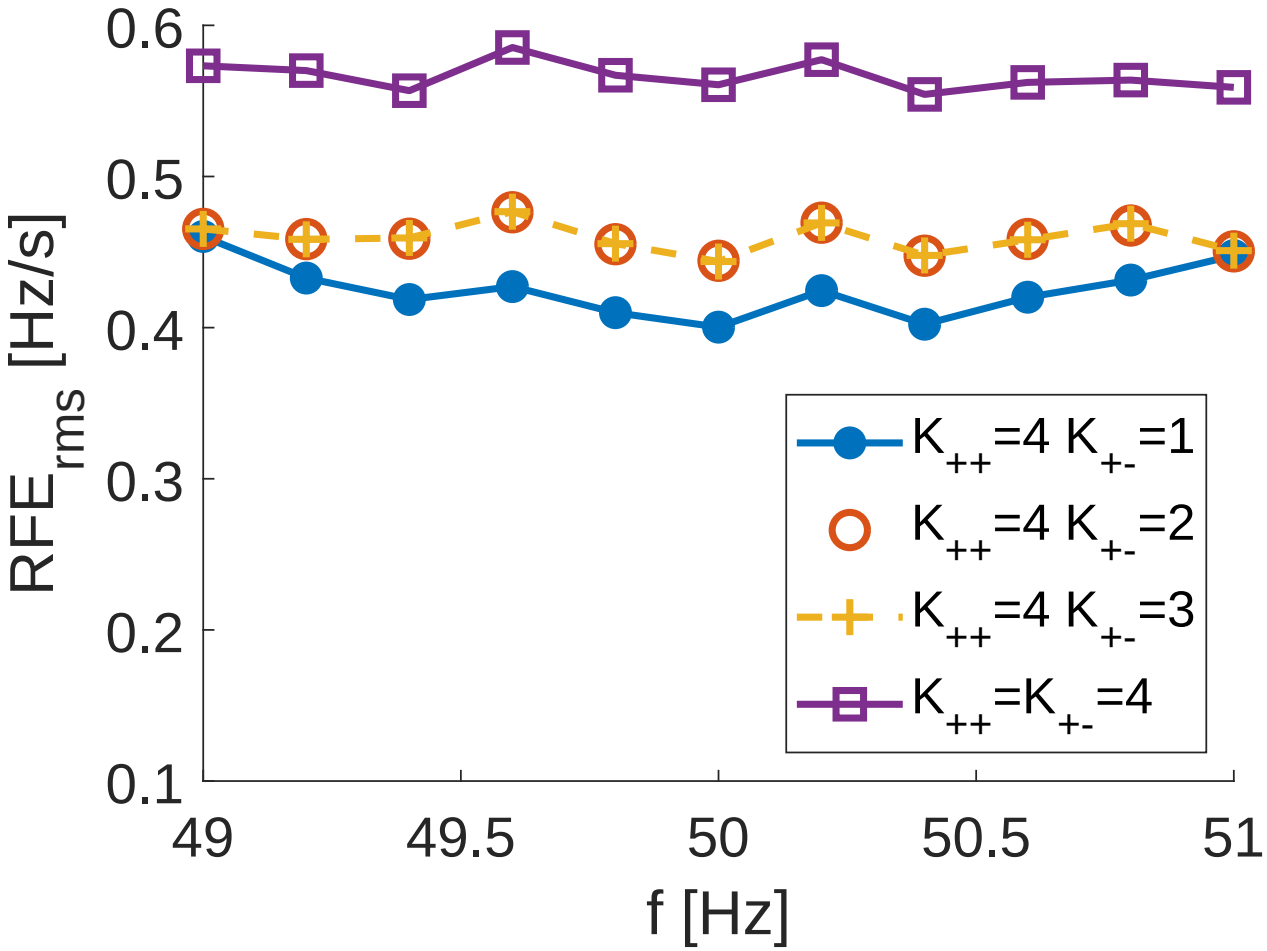

Fig. 4. Root mean square RFE achieved by SV-TF with different negative sequence component expansion orders under magnitude unbalance, 60 dB SNR.

TABLE IV
ROOT MEAN SQUARE TVE OF $\bar{X}_-$ ESTIMATION UNDER MAGNITUDE UNBALANCE ($\delta_m = +10\,\%$). SNR = 60 dB

Orders		**TVE** [%]	
K_{-+}	K_{--}	**50 Hz**	**49 Hz**
1	1	0.194	0.443
2	2	0.291	0.293
2	1	0.194	0.314
3	3	0.295	0.295
3	2	0.294	0.294
3	1	0.198	0.303
4	4	0.381	0.379
4	3	0.306	0.305
4	2	0.305	0.305
4	1	0.202	0.290

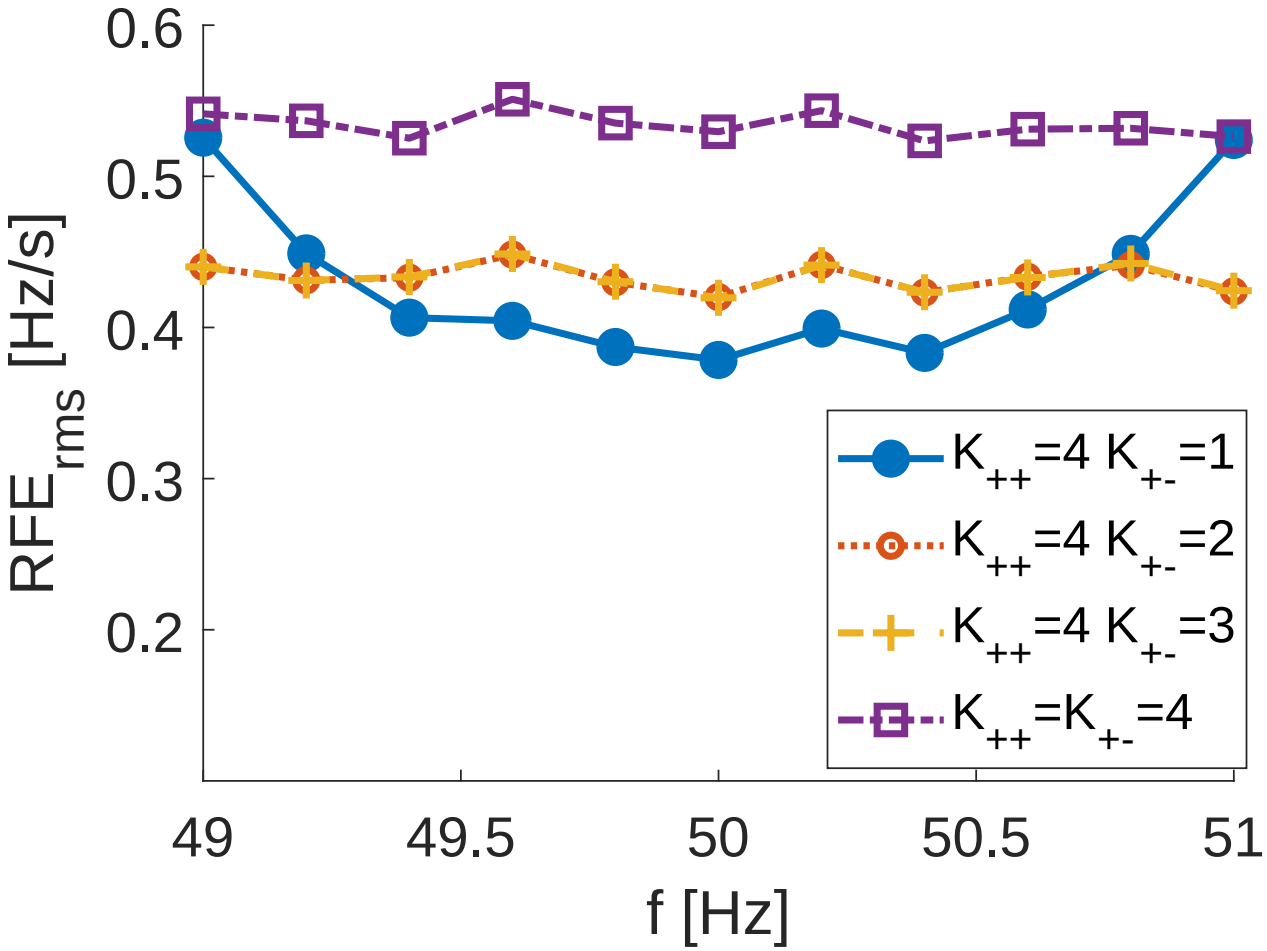

Fig. 5. Root mean square RFE achieved by SV-TF with different negative sequence component expansion orders under phase unbalance, 60 dB.

Simultation results have shown that the proposed method allows following positive and negative sequence synchrophasors, frequency and ROCOF dynamics with remarkable accuracy both in presence of noise and under off-nominal frequency conditions. The higher flexibility allowed by the three-phase approach permits better performance with respect to the conventional *per-phase* TF expansion.

The proposed framework is intended to permit a fine-tuning of PMU design that allows a better exploitation of the peculiarities of three-phase signals, which is extremely promising for many important applications requiring accurate estimates of the symmetrical components.

Acknowledgments

Dr. Pegoraro's work was partially funded by Fondazione di Sardegna for the research project "SUM2GRIDS, Solutions by mUltidisciplinary approach for intelligent Monitoring and Management of power distribution GRIDS".

References

[1] A. G. Phadke and J. S. Thorp, *Synchronized Phasor Measurements and Their Applications*. Springer Science, 2008.
[2] AA. VV., *Phasor Measurement Units and Wide Area Monitoring Systems*, 1st ed., A. Monti, C. Muscas, and F. Ponci, Eds. Academic Press, 2016.
[3] *IEEE Standard for Synchrophasor Measurements for Power Systems*, IEEE IEEE Std C37.118.1-2011 (Revision of IEEE Std C37.118-2005), Dec. 2011.
[4] *IEEE Standard for Synchrophasor Measurements for Power Systems – Amendment 1: Modification of Selected Performance Requirements*, IEEE IEEE Std C37.118.1a-2014 (Amendment to IEEE Std C37.118.1-2011), Apr. 2014.
[5] J. A. de la O Serna, "Dynamic phasor estimates for power system oscillations," *IEEE Trans. Instrum. Meas.*, vol. 56, no. 5, pp. 1648–1657, Oct. 2007.
[6] W. Premerlani, B. Kasztenny, and M. Adamiak, "Development and implementation of a synchrophasor estimator capable of measurements under dynamic conditions," *IEEE Trans. Power Del.*, vol. 23, no. 1, pp. 109–123, Jan. 2008.
[7] R. K. Mai, Z. Y. He, L. Fu, B. Kirby, and Z. Q. Bo, "A dynamic synchrophasor estimation algorithm for online application," *IEEE Trans. Power Del.*, vol. 25, no. 2, pp. 570–578, Apr. 2010.
[8] D. Petri, D. Fontanelli, and D. Macii, "A frequency-domain algorithm for dynamic synchrophasor and frequency estimation," *IEEE Trans. Instrum. Meas.*, vol. 63, no. 10, pp. 2330–2340, Oct. 2014.

[9] P. Castello, J. Liu, C. Muscas, P. A. Pegoraro, F. Ponci, and A. Monti, "A fast and accurate PMU algorithm for P+M class measurement of synchrophasor and frequency," *IEEE Trans. Instrum. Meas.*, vol. 63, no. 12, pp. 2837–2845, Dec. 2014.

[10] S. Toscani and C. Muscas, "A space vector based approach for synchrophasor measurement," in *Instrum. and Meas. Technol. Conf. (I2MTC) Proc., 2014 IEEE Int.*, May 2014, pp. 257–261.

[11] S. Toscani, C. Muscas, and P. A. Pegoraro, "Design and performance prediction of space vector-based pmu algorithms," *IEEE Trans. Instrum. Meas.*, vol. 66, no. 3, pp. 394–404, Mar. 2017.

[12] R. Ferrero, P. A. Pegoraro, and S. Toscani, "Employment of interpolated DFT-based pmu algorithms in three-phase systems," in *Proceeding of the IEEE International Workshop on Applied Measurements for Power Systems (AMPS)*, Liverpool, UK, Sep. 2017.

[13] L. Zhan, Y. Liu, and Y. Liu, "A Clarke transformation-based DFT phasor and frequency algorithm for wide frequency range," *IEEE Transactions on Smart Grid*, vol. 9, no. 1, pp. 67–77, Jan 2018.

[14] Y. Xia, S. Kanna, and D. P. Mandic, "Maximum likelihood parameter estimation of unbalanced three-phase power signals," *IEEE Transactions on Instrumentation and Measurement*, vol. 67, no. 3, pp. 569–581, Mar. 2018.

[15] F. Messina, P. Marchi, L. R. Vega, C. G. Galarza, and H. Laiz, "A novel modular positive-sequence synchrophasor estimation algorithm for pmus," *IEEE Transactions on Instrumentation and Measurement*, vol. 66, no. 6, pp. 1164–1175, June 2017.

[16] P. Castello, R. Ferrero, P. A. Pegoraro, and S. Toscani, "Synchrophasor and frequency estimations: Combining space vector and Taylor-Fourier approaches," in *2018 IEEE International Instrumentation and Measurement Technology Conference (I2MTC)*, May 2018, pp. 1–6.

[17] N. C. Woolley and J. V. Milanovic, "Statistical estimation of the source and level of voltage unbalance in distribution networks," *IEEE Transactions on Power Delivery*, vol. 27, no. 3, pp. 1450–1460, July 2012.

[18] T. Routtenberg, Y. Xie, R. M. Willett, and L. Tong, "PMU-based detection of imbalance in three-phase power systems," *IEEE Transactions on Power Systems*, vol. 30, no. 4, pp. 1966–1976, July 2015.

[19] M. Brown, M. Biswal, S. Brahma, S. J. Ranade, and H. Cao, "Characterizing and quantifying noise in pmu data," in *2016 IEEE Power and Energy Society General Meeting (PESGM)*, July 2016, pp. 1–5.

[20] *IEEE Guide for Synchronization, Calibration, Testing, and Installation of Phasor Measurement Units (PMUs) for Power System Protection and Control*, IEEEC37.242-2013, Mar. 2013.

[21] OMICRON, *CMC 256Plus Technical Data*. [Online]. Available: https://www.omicronenergy.com/en/download/document/69C95E19-2233-4610-B86E-CA2C87DBBBA8/

[22] OMICRON, *CMIRIG-B Technical Data*. [Online]. Available: https://www.omicronenergy.com/en/download/document/4EC4E377-7BEB-4749-964B-51D64AC5CC0F/

[23] National Instruments, *NI-9225 Specifications*. [Online]. Available: http://www.ni.com/pdf/manuals/374707e.pdf

Paolo Castello (S'11M'15) received the M.S. degree in Electronic Engineering and the Ph.D. degree in Electronic and Computer Engineering from the University of Cagliari in 2010 and in 2014, respectively. Currently, he is assistant professor in the Electrical and Electronic Measurements Group of the Department of Electrical and Electronic Engineering at the University of Cagliari. His research activity focuses on the development of algorithms for synchrophasor calculation, the characterization and testing of Phasor Measurement Units, and design of new monitoring architectures for power systems based on IEC 61850 standard.

Roberto Ferrero (S10-M14-SM18) received his PhD degree (cum laude) in Electrical Engineering from Polytechnic of Milan, Italy, in 2013. He has been a lecturer with the Department of Electrical Engineering and Electronics, University of Liverpool, UK, since 2015. His main research activity is focused on electrical measurements, particularly applied to power systems and electrochemical devices. He is a member of the IEEE Instrumentation and Measurement Society, and of its TC 39 (Measurements in Power Systems). He has been an Associate Editor of the IEEE Transactions on Instrumentation and Measurement since 2017.

Paolo Attilio Pegoraro (M06) received the M.S. (summa cum laude) degree in telecommunications engineering and the Ph.D. degree in electronic and telecommunications engineering from the University of Padova, Padua, Italy, in 2001 and 2005, respectively. From 2015 to 20018, he was an Assistant Professor with the Department of Electrical and Electronic Engineering, University of Cagliari, Cagliari, Italy, where he is currently Associate Professor. He has authored or co-authored over 80 scientific papers. His current research interests include the development of new measurement techniques for modern power networks, with attention to synchronized measurements and state estimation for distribution grids. Dr. Pegoraro is a member of the IEEE Instrumentation and Measurement Society and of its TC 39 (Measurements in Power Systems).

Sergio Toscani (S08, M12) received the M.Sc. (cum laude) and the Ph.D degree in electrical engineering from the Politecnico di Milano, Milan, Italy, in 2007 and 2011 respectively. Since 2011 he is Assistant Professor in Electrical and Electronic Measurement with the Dipartimento di Elettronica, Informazione e Bioingegneria of the same University. His research activity is mainly focused on development and testing of current and voltage transducers, measurement techniques for powers systems, electrical components and systems diagnostics. Dr. Sergio Toscani is member of the IEEE Instrumentation and Measurement Society and of the TC-39 - Measurements in Power Systems.